

# The Power State Estimation Method for High Energy Ternary Lithium-ion Batteries Based on the Online Collaborative Equivalent Modeling and Adaptive Correction - Unscented Kalman Filter

Yongcun Fan<sup>1</sup>, Shunli Wang<sup>1,\*</sup>, Cong Jiang<sup>1</sup>, Carlos Fernandez<sup>2</sup>

<sup>1</sup> School of Information Engineering, Southwest University of Science and Technology, Mianyang, 621010, China

<sup>2</sup> School of Pharmacy and Life Sciences, Robert Gordon University, Aberdeen AB17GJ, UK.

\*E-mail: [497420789@qq.com](mailto:497420789@qq.com)

Received: 19 September 2020 / Accepted: 5 November 2020 / Published: 30 November 2020

---

Accurate power state estimation plays an important role in the real-time working state monitoring and safety control of high energy lithium-ion batteries. To solve the difficulty and low accuracy problems in its real-time power state estimation under various operating conditions, the working characteristics of the lithium cobalt oxide batteries are analyzed comprehensively under various operating conditions. An improved collaborative equivalent model is established to characterize its working characteristics and then the initial power state value is calibrated by using the experimental relationship between open circuit voltage and state of charge considering the importance of the precious estimation accuracy for the later iterate calculation and correction. And then, an adaptive correction - Unscented Kalman Filter algorithm is put forward and applied for the state of charge estimation and output voltage tracking so as to realize the real-time high-precision lithium-ion battery power state estimation. The experimental results show that the established model can predict the power state of high energy lithium-ion batteries conveniently with high convergency speed within 30 seconds, accurate output voltage tracking effect within 32 mV and high accuracy, the max estimation error of which is 3.87%, providing an effective working state monitoring and safety protection method in the cleaner production and power supply processes of the high energy lithium-ion batteries.

---

**Keywords:** high energy lithium-ion battery; collaborative equivalent model; power state estimation; adaptive correction - Unscented Kalman Filter; output voltage tracking

## 1. INTRODUCTION

With the large-scale promotion and application of new energy vehicles and large scale energy distribution, the power source demand is increasing for the high energy lithium-ion batteries with high

specific energy, small size, and rechargeability advantages, which have gradually become the preferred power supply sources of new energy storage [1]. Lithium-ion batteries are regarded as the key energy storage technology for both e-mobility and stationary renewable energy storage applications [2]. Its outstanding advantages are expressed as low-weight, high energy storage, less pollution, no memory effect, and longer service life. What is more, lithium-ion batteries have 1.6 times more energy storage than hydrogen nickel batteries and 4 times more energy storage than nickel cadmium batteries at the same volume and weight [3]. However, it has been found that lithium batteries themselves consume a lot of energy overtime during the operation process due to the internal resistance and other time-varying parameters [4], which are the key factors that determine the current state of this kind of electrochemical storage systems.

As joule heat and resistance are proportional to each other when current and time are constant, the lithium battery consumes more energy by itself along with greater internal resistance [5]. Consequently, the diagnosis of cell degradation is necessary for reliable and safe operation of lithium-ion batteries in electric or hybrid vehicles [6]. This can be achieved by monitoring the increase of the internal resistance in the battery cells over the whole lifetime of the battery. Therefore, it cannot be waited to try our best to reduce the internal resistance of lithium battery to save energy and it is necessary to have an experimental test about how the internal resistance of lithium battery changes towards its surroundings [7]. The state of charge can reflect the remaining capacity of the battery which also affects the internal resistance of the lithium-ion batteries [8]. As this is a complicated reaction progress, the battery internal parameters have different effects on its internal resistance [9]. What is more, the lithium-ion battery itself has a complicated internal structure that is affected by the state of charge, current and pulse time, and the age of the battery itself. Hence, this experiment needs to use the control variables to discover per variable of the three variables on how to affect the internal resistance [10, 11]. Besides, it is necessary to use several new batteries with the same initial internal resistance under different temperature situations.

The internal resistance of battery is a very important indicator to measure its health state at the different current, power state, and pulse time working conditions [12]. Through drawing and analysis, the change of internal resistance can be obtained under different conditions to provide data for describing the battery performance, in which the internal resistance characteristics of the lithium-ion batteries are tested by using the hybrid pulse power characterization method [13, 14], the relationship of which is considered and analyzed for the capacity, internal resistance, state of charge and pulse current, and properties of the capacity. And then, the ohmic resistance is obtained for the batteries, providing the basis of online resistance identification and peak power computation for the battery packs [15]. Due to the complex internal structure of the high energy lithium-ion batteries, the experimental data often shows strong nonlinear characteristics in its charge-discharge working process, which makes it difficult for traditional power state estimation algorithms to obtain its real-time and accurate state of charge estimation values [16-18]. Consequently, the extended and unscented Kalman filters are introduced into the iterate calculation process of the power state estimation, which are based on the Kalman filtering algorithm, aiming to solve the problems of large errors and slow convergence speed brought by the nonlinear battery characteristics in the state of charge estimation process [19-21].

The power state estimation methods mainly include impedance test, Ampere-hour integral, open circuit voltage, electromotive force, etc. The Ampere-hour integral method requires high precision current measurement and calibration initial power state value [22, 23], which is difficult to guarantee in practical power supply applications. The open circuit voltage method relies on its curve relationship towards the residual energy level of lithium-ion batteries to calculate its power state values [24-26]. In addition, the voltage of the battery needs to be measured after long-term stowing, which is difficult to be realized in practical power supply applications. The impedance measurement method calculates the power state values according to the alternating current impedance [27-29], while the alternating current impedance of the battery varies little in the middle range of power state value and its error is large [30-33]. As a result, the potential method calculates the electromotive force based on the current value and terminal voltage flowing through the lithium-ion batteries by substituting it into the equivalent circuit model [34-36], and then it looks up the power state value according to the open circuit voltage curve towards different state of charge levels. A variety of experimental methods are integrated, including hybrid power charge-discharge, constant voltage charge towards different multiplicity, and constant exile experiments [37-39]. Cyclic discharge experiments are shelved to study and analyze the working characteristics of lithium-ion batteries, in which the response characteristics of battery are discussed and analyzed under different working conditions. Then, the equivalent circuit model is established by using the hybrid pulse power test to identify its parameters [40-42], which is also used to determine the relationship between the model parameters and state of charge changes in lithium-ion batteries under different charging and discharging stages [43, 44]. The equivalent model is established with dynamic parameters of the lithium-ion battery and the model verification can fully characterize its working state [45-47].

As the accuracy of this method depends on the accurate initial power state value, an improved collaborative equivalent model is built that is based on ampere-hour, open circuit voltage, and other equivalent circuit modeling methods. The equivalent circuit model is established firstly, which is then carried out in the hybrid power charge and discharge experiments, and then the model parameters are identified off-line by analyzing the experimental data, which is conducted and established to realize the modeling research on the lithium-ion battery power state estimation to solve the difficult problems in the real-time state of charge estimation with high accuracy. Moreover, the related power state estimation problems of lithium-ion batteries are solved by the equivalent circuit modeling that is combined with the Adaptive Correction - Unscented Kalman Filter (AC-UKF) algorithm. According to the experimental data, a simulation model is established to check the model accuracy and power state estimation effect, in which the equivalent model can simulate the characteristics of batteries and improve the power state estimation accuracy effectively that is suitable for the online power state estimation of the high energy lithium-ion batteries. The comprehensive analysis consists of a variety of lithium-ion battery charged state estimation algorithm, in which the open circuit voltage is used to estimate the initial value for the calibration, and the Kalman filtering calculation is then investigated for its real-time state of charge estimation with lithium-ion battery power state modeling.

## 2. MATHEMATICAL ANALYSIS

The AC-UKF algorithm is used to estimate the power state of lithium-ion batteries and a relatively accurate model was obtained, in which the adaptive resistance-capacitance equivalent circuit model is adopted to record the experimental data of hybrid pulse power charge-discharge for the battery data processing. It is an optimized autoregressive data processing algorithm, which is not only suitable for the stationary processes but also the non-stationary processes. In addition, it can be investigated with good real-time performance and easy implementation characteristics with a strong dependence on the model. Therefore, its state and observation equations can be obtained by writing algorithm program, according to which the error estimation and comparative analysis of its estimated and actual values in different working conditions are conducted. The power state estimation investigated by this algorithm can effectively reduce system errors and correct the initial power state value deviation. As for this typical nonlinear system, its state and measurement equations are shown in Eq. (1).

$$\begin{cases} X_k = f(X_{k-1}, U_k) + W_k \\ Y_k = g(X_{k-1}) + V_k \end{cases} \Rightarrow \begin{cases} x_k = A_{k-1}x_{k-1} + B_{k-1}u_{k-1} + w_{k-1} \\ y_k = C_{k-1}x_k + D_k u_k + w_k \end{cases} \quad (1)$$

Wherein,  $k$  is the time moment and  $f(x_{k-1}, U_k)$  is the nonlinear system state transfer equation.  $g(x_{k-1})$  is the nonlinear measurement equation, in which  $X_k$  is the state variable and  $U_k$  is the known input. And then,  $Y_k$  is taken as the measurement signal. In order to represent the noise influence,  $W_k$  is used as the process noise and  $V_k$  is taken as the measurement noise, the relationship of which is assumed to be unrelated.  $x_k$  represents the system state variable at time  $k$ , and  $y_k$  is the system observed variable at time  $k$ . Meanwhile,  $u_k$  is the system input that is used as the control variable.  $A_k$  is the transfer matrix of state  $x$  from  $k-1$  to  $k$ , and  $B_k$  is the input matrix.  $C_k$  is the measurement matrix and  $D_k$  is the feedforward matrix.  $\omega_k$  is the noise of the system state equation named as the process noise, whose variance is  $Q_k$ .  $v_k$  is the noise of the measurement equation named as the observed noise, whose variance is  $R_k$ . The mean values are both zero gaussian white noise, and their covariances are  $Q_w$  and  $R_v$  respectively. The specific iterate calculation process is designed, in which the initial parameter state value is described as shown in Eq.(2).

$$\begin{cases} \bar{x} = E(x_0), P_0 = E(x_0 - \bar{x}) \\ y^i_{k/k-1} = g(x^i_{k/k-1}), \bar{y}_k = \sum_{i=0}^{2L} w_i^m [g(x^i_{k/k-1}) + v_{k-1}^i] = \sum_{i=0}^{2L} w_i^m y^i_{k/k-1} \end{cases} \quad (2)$$

Establishing reasonable state and observation equations based on an accurate battery model is essential. However, since the battery system exhibits strong nonlinearity, the Kalman filtering algorithm is not ideal for this nonlinear power state estimation process [48]. Therefore, the improved calculation treatment is investigated to linearize the nonlinear system through Taylor expansion. Subsequently, the established Sigma data points are described as shown in Eq.(3).

$$\begin{cases} x^i_{k-1} = \bar{x}_{k-1} + \left[ \sqrt{(L + \lambda)P_{k-1}} \right]_i, i = 1, \dots, L \\ x^i_{k-1} = \bar{x}_{k-1} - \left[ \sqrt{(L + \lambda)P_{k-1}} \right]_i, i = L + 1, \dots, 2L + 1 \end{cases} \quad (3)$$

The prediction, feedback, correction, and update are performed cyclically, according to which the process data can be analyzed. The Kalman gain is updated dynamically that is based on the error covariance of the state variables and the observed variables, according to which the state variables are updated iteratively based on the estimated errors of the observed variables. Compared with other

algorithms, it is simpler and easier to be investigated, the filtering effect of which is stable and reliable, making its application range to be quite wide. According to the classical Kalman filter algorithm, the power state estimation algorithm is derived by combining the UKF and adaptive Kalman filter together that relies on the calculation improvements and introduced by some defects, the state update equation of which is shown in Eq.(4).

$$\begin{cases} x_{k/k-1}^i = f(x_{k-1}^i), \bar{x} = \sum_{i=0}^{2L} \omega_i^m x_{k/k-1}^i \\ P_{k/k-1} = \sum_{i=0}^{2L} \omega_i^c (x_{k/k-1}^i - \bar{x}_k)(x_{k/k-1}^i - \bar{x}_k)^T + Q_k \\ y_{k/k-1}^i = g(x_{k/k-1}^i), y_k = \sum_{i=0}^{2L} \omega_i^m [g(x_{k/k-1}^i + v_{k-1}^i)] = \sum_{i=0}^{2L} \omega_i^m y_{k/k-1}^i \end{cases} \quad (4)$$

In the equation,  $k/k-1$  is the estimated power state value of the time point  $k$  based on the obtained power state value at time point  $k-1$ . As the iterate calculation algorithm is a nonlinear process, the observation value of the system input and output should be applied to update continuously to achieve the optimal internal resistance estimation that is conducted by estimating the state value of the next time moment from the previous time. When it is used to estimate the power state of a lithium-ion battery, the process noise and the observed noise are required to be white noise with a Gaussian distribution, which is a limitation of the Kalman filtering based methods. The Taylor expansion algorithm is applied to unfold the system model of the lithium-ion battery. Then, the first-order linearization model is left when the high-order terms are removed. The measurement update equation is shown in Eq.(5).

$$\begin{cases} P_{k/k-1} = \sum_{i=0}^{2L} \omega_i^c (x_{k/k-1}^i - \bar{x}_k)(x_{k/k-1}^i - \bar{x}_k)^T + Q_k \\ P_{x,y,k} = \sum_{i=0}^{2L} \omega_i^e (x_{k/k-1}^i - \bar{x}_k)(y_{k/k-1}^i - \bar{y})^T \\ K = P_{x,y,k} P_{y,k}^{-1}, \bar{x}_k = \bar{x}_{k-1} + K(y_k - \bar{y}_{k-1}), P_{k/k-1} = P_{k/k-1} - K P_{y,k}^{-1} K^T \end{cases} \quad (5)$$

The iterate calculation process can be realized by repeating the above four steps, according to which the optimal state  $X_k$  at time point  $k$  can be estimated as long as the initial conditions of  $X$  and  $P$  are given. According to the state value at time point  $k-1$ , the input, and observed values at time point  $k$  can be acquired. At the time point of  $k$ , it is assumed that the covariance of the  $k-1$  state estimation values and the estimation errors at the previous time has been obtained. The power state value at time point  $k$  is predicted in advance by the state values of the  $k-1$ -time moment. In the mathematical model, the latter time moment is a function of the previous time moment.

### 2.1. Collaborative equivalent modeling

The collaborative equivalent model is combined with the hybrid pulse power test, in which the capacitor  $C_b$  is used to describe the battery open circuit voltage changes,  $U_{OC}$  is the ideal voltage source,  $R_o$  is the ohm resistance,  $R_p$  is the polarization resistance,  $C_p$  is the polarization capacitance. The battery polarization process is reflected through the parallel circuit of  $R_p$  and  $C_p$ , thus greatly reducing the battery

polarization effect caused by the production process and the working environment influence.  $E$  represents the electromotive force of the power supply and is taken as an ideal voltage source.  $C_b$  represents the open circuit voltage change caused by the accumulation of power supply current,  $I$  is the current in the battery loop,  $U_L$  represents the battery terminal voltage.  $E$  and  $C_b$  are combined together to represent the battery open circuit voltage change.

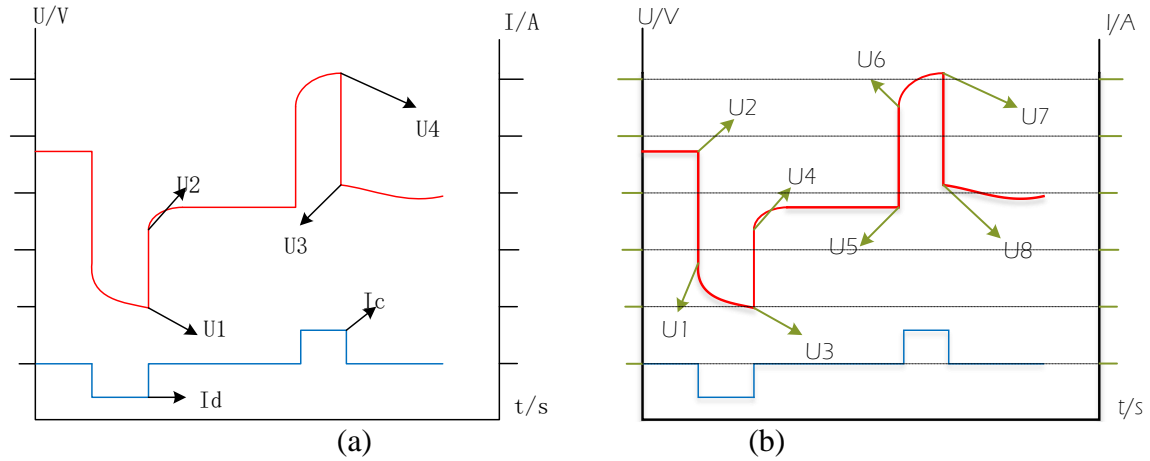


**Figure 1.** Collaborative equivalent modeling effect characterization

According to the model column of the Kirchhoff current and voltage law circuit equations, the model parameters are identified by combining the internal characteristics of the battery cell reflected by the hybrid pulse power characteristic (HPPC) experiments. As there is a great deal of difference between internal connected battery cells, such as voltage, capacity, and temperature, which increases along with the battery aging process, the self-discharge and temperature influencing effect are considered in this model. By analyzing the illustrated equivalent circuit model, the state-space equation of each parameter can be obtained as shown in Eq.(6).

$$U_L = U_{OC} - C_b \left( \int i(t) dt \right) - R_o I_L - R_p I_p \tag{6}$$

In the hybrid pulse power experimental test of model parameter identification, four different sampling time points of  $a$ ,  $b$ ,  $c$ , and  $d$  are selected for the mathematical description of its state-space equations. Wherein,  $U_{OC}$  represents the open circuit voltage,  $R_o$  represents the internal resistance,  $R_p$  represents the polarization resistance,  $C_p$  represents the polarization capacitance,  $I_L$  represents the load current and its value equals to  $I$ ,  $I_p$  represents the current through the polarization internal resistance, and  $U_L$  represents the closed voltage of the external load. And the subscript parameters of  $a$ ,  $b$ ,  $c$ , and  $d$  are used to represent the state values of model parameters at different time points. The change rule of each parameter was obtained by HPPC experiment, and the current and voltage change were set as shown in Figure 1.

By analyzing the diagram, the conclusions can be as follows. (1)  $U1 \sim U2$ : The voltage transient is caused by the ohmic internal resistance  $R_o$ , and the voltage drops from  $U1$  to  $U2$ . (2)  $U2 \sim U3$ : The polarization capacitor  $C_p$  in the RC network is charged, and the voltage is slowly decreased to form a zero-input response. (3)  $U3 \sim U4$ : At this time point, the current is abrupt, the current suddenly changes

to 0, and the voltage drop on the ohm internal resistance disappears, causing the voltage transient to rise. (4) U4~U5: At this time, the polarization capacitor  $C_s$  is discharged through the polarization internal resistance  $R_2$ , and the voltage slowly rises. According to the above analysis, each parameter can be identified as shown below.

To measure the battery internal resistance accurately, an appropriate measurement should be conducted and there are many methods for measuring the internal resistance of the battery, including the alternating current internal resistance test, the direct current internal resistance test method, and so on [49]. Test equipment forces the battery to pass a large constant current for a short time and the voltage change across the battery are measured in this case at the same time, according to which the ohm formula is used subsequently to calculate the battery internal resistance. The ohmic internal resistance calculation formula should be designed as well as its corresponding weights. The zero-input response expression for the resistance-capacitance network is also designed together with the open circuit voltage calculation, in which the time constant is calculated. In the hybrid pulse power experimental voltage change curve, the voltage drops linearly from  $U_1$  to  $U_2$  at time point  $t_1$  is mainly because of the ohmic internal resistance that is obtained as shown in Eq.(7).

$$\begin{cases} R_o = \frac{\Delta U}{I} = \frac{U_1 - U_2}{I}, \tau = -\frac{t_4 - t_3}{\ln\left(\frac{U_1 - U_4}{U_1 - U_3}\right)}, U_p = U_1 e^{-\frac{t}{\tau}} \\ R_p = \frac{\Delta U'}{I} = \frac{U_5 - U_4}{I}, U_{oc} = U_1 - U_p = U_1 \left(1 - e^{-\frac{t}{\tau}}\right) \end{cases} \quad (7)$$

Wherein,  $I$  is the hybrid pulse power current in the charge-discharge testing process. The extended Kalman filter algorithm is based on the ordinary Kalman filter algorithm, which is a technique for online linearization. This means linearizing the estimated parameters and then performing linear Kalman filtering, thereby achieving an accurate internal resistance estimation of the lithium-ion battery. In this case, the system noise and process noise are generally approximated as white noise in accordance with a Gaussian distribution [50]. The Kalman filter linearizes the expectation and covariance of system and process noises during the estimation process. By measuring the voltage in the charge and discharge test, the charge and discharge resistances under different charge states are respectively determined, the calculation formula of which is shown as follows.

$$\begin{cases} R_d = (U_2 - U_1) / I_d \\ R_c = (U_4 - U_3) / I_c \end{cases} \quad (8)$$

Among them,  $R_d$  stands for the discharge resistance and  $R_c$  stands for the charge resistance.  $I_d$  represents the discharge pulse current and  $I_c$  represents the charge pulse current. The characteristics of direct current internal resistance test method are obtained accordingly. This measurement method has higher precision, which can test large capacity batteries with high current of 40~80 A within 2~3 s. The alternating current internal resistance measurement can be conducted in the offline parameter identification, in which the battery is actually equivalent to the power supply resistor. Therefore, an alternating signal with a natural frequency and a fixed current is applied to the lithium-ion battery and its voltage is measured subsequently after a series of rectification and filtering processes [51, 52], in which the internal resistance of the battery is calculated through an operational amplifier circuit. This

test method is to apply a current of 1~5 s to  $I_a$ , and the current of 1 k HZ is investigated on the battery. The open circuit voltage change  $C_b$  is caused by the accumulation of power supply current, the calculation process of which is shown in Eq.(9).

$$C_b = \frac{\int_{t_1}^{t_3} idt}{U_1 - U_5} = \frac{(t_2 - t_1)I}{U_1 - U_5} \quad (9)$$

In the HPPC experiment,  $t_1$  to  $t_2$  is a constant discharge process of  $I$ , and  $t_2$  to  $t_3$  is the shelving stage as expressed in the formula. Since the polarization effect of the cell starts from  $t_1$ ,  $t_1$  to  $t_2$  is the zero-state response process of the resistance-capacitance circuit. The Kalman filter algorithm uses the linear state equation to estimate the current system state by inputting and outputting data [53]. Because it is completely estimated at the time domain, there is no mutual conversion to realize the translation treatment between the time domain and the frequency domain [54, 55], so the calculation amount is small and the real-time estimation effect is quite good. The classical Kalman filter algorithm is just suitable for the linear systems, while the lithium-ion battery internal resistance system is nonlinear. The extended Kalman filter algorithm is an improvement to the classical Kalman filter algorithm [56], which is to spread the nonlinear space equation through Taylor, round off the second-order and above high-order terms to obtain the approximate linear space equation. And then, the traditional Kalman filter algorithm is applied to the linear space equation to estimate the current spatial state, which is suitable for the discrete non-distribution linear system [57]. The expression equations and observation equations of the discrete nonlinear system space can be obtained accordingly. Therefore,  $R_p$  is obtained for the polarization resistance identification as shown in Eq.(10).

$$E = U_2 - \frac{\int_{t_1}^{t_3} idt}{C_b} - iR_p(1 - e^{-\frac{t}{\tau}}) \quad (10)$$

Just for the polarization capacitance identification, it can be transformed in a first order resistance-capacitance circuit time constant  $\tau = R_p C_p$ . For the nonlinear problem of lithium batteries, it does not adopt the way of forced linearization of the system, but obtains a certain number of sampling points near the state estimation according to the sampling theorem of the statistical principle. The sampling point is usually called the Sigma point, which needs to satisfy the condition that it has the same mean value and covariance as the original state to ensure the transitivity to the original state. Then, the Sigma point set is nonlinearly transmitted using the state equation, and the transformed mean is obtained, and the optimal solution is obtained in the iterative process. This approximation is essentially a statistical approximation rather than a solution but has a higher computational accuracy for the statistics of nonlinear distributions. In the experimental HPPC, the formulas for calculating  $\tau$  and  $C_p$  are computed as shown in Eq.(11).

$$\tau = -\frac{t_3 - t_2}{\ln \frac{U_1 - U_4}{U_1 - U_3}} \Rightarrow C_p = -\frac{t_3 - t_2}{R_p \ln \frac{U_1 - U_4}{U_1 - U_3}} \quad (11)$$

In combination with these equations, the values of  $R_o$ ,  $C_b$ ,  $R_p$ , and  $C_p$  can be obtained. The commonly used measurement methods of lithium-ion battery internal resistance include the volt-ampere characteristic curve method, density method, open circuit voltage method, alternating current injection method, direct current discharge method, and HPPC test method. The comprehensive comparison shows

that the HPPC method is simple to implement and can accurately obtain the ohm internal resistance and polarization internal resistance of lithium-ion batteries at different power state values. Therefore, the internal resistance of the lithium-ion battery was obtained by using the HPPC method, and then the experimental current and voltage curve of HPPC is obtained. The HPPC experiment is to conduct pulse charge and discharge on the tested battery, and simultaneously detect the instantaneous voltage change at both ends of the battery, so as to estimate the ohm resistance and polarization resistance of the lithium-ion battery. The current and voltage changes of a single HPPC experiment are shown in Figure 2.

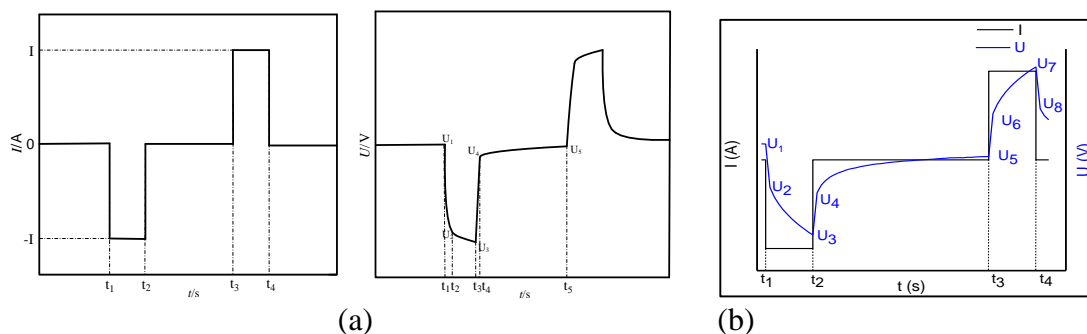


**Figure 2.** hybrid pulse power characteristics

Wherein, the black curve is the current curve and the blue curve is the voltage curve. In the HPPC experiment,  $t_1$  to  $t_2$  is constant discharge time of 10s, then  $t_2$  to  $t_3$  is shelving time of 40 s, followed by constant current charge time of  $t_3$  to  $t_4$  of 10s. Exile from  $t_1$  time constant power, make the voltage of the lithium-ion battery quickly decreased from  $U_1$  to  $U_2$ , due to polarization effect, the voltage decline slower and slower, continues with the discharge process, the voltage slowly decreased from  $U_2$  to  $U_3$ ,  $t_2$  time stop after discharge, the terminal voltage has rapidly risen from  $U_3$  to  $U_4$  first, then the same as the polarization effect, up from  $U_4$  to  $U_5$  rate slower and slower, charging process is similar. According to the experimental schedule, the HPPC tests are carried out for lithium-ion batteries and the charging and discharging rate was set as 50A (1C) at a total of 10 points. The working steps of a single cycle were 10s constant discharge electric pulse, 40s shelving, 10s constant current charging pulse, and the interval between 10 power state pulse cycles was one hour. The current pulse curve and corresponding voltage change curve in the HPPC experiment is used in the parameter identification process.

As can be known from the voltage response curve of HPPC experimental cells, features can be extracted and calculated to obtain the model parameters of 10 power state points, which are characterized as follows. (1) discharge start time  $t_1$  and discharge stop time  $t_2$  voltage vertical change is due to the existence of the battery ohm resistance caused by the voltage transient. (2) during  $t_1 \sim t_2$ , the terminal voltage of the battery slowly drops, which is the process of discharging current charging the polarization capacitor and is the zero-state response of the double resistance-capacitance series circuit. (3) during  $t_2 \sim t_3$ , the terminal voltage of the battery rises slowly, which is the process of the polarization capacitor discharging to the polarization resistance and is the zero-input response of the double resistance-capacitance series circuit. (4) the battery terminal voltage  $U_1$  before the discharge pulse is slightly higher

than the terminal voltage  $U_5$  when the discharge ends and reaches a stable state, which is the voltage difference caused by the discharge current integrating on the energy storage capacitor.

As can be seen from the above characteristics, the improved model  $R_o$  and  $C_b$  value can be directly from the characteristics (1) and (4). The polarization resistance and polarization capacitance values in the double resistance-capacitance circuit can be identified according to the voltage curve of characteristic (2) and (3). The open circuit voltage  $U_{OC}$  is the stable voltage between the positive and negative ends of the battery under a long standing state. The experiment shows that the terminal voltage of the battery after standing for 1 h is basically equal to the open circuit voltage of the battery. Therefore, the battery is kept at 1C multiplier for 6 min and then set aside for 1 h. At this time, the voltage at both ends of the battery is the open circuit voltage of the lithium-ion battery in the corresponding power state. The sudden changes in the terminal voltage of the battery at the moment of discharge and the moment of the stop are all caused by ohm internal resistance, so the value of ohm internal resistance can be calculated by ohm's law, as shown in Eq.(12).

$$R_o = \frac{(U_1 - U_2) + (U_4 - U_3)}{2I} \quad (12)$$

The improved model is a typical double resistance-capacitance circuit model, in which the HPPC experiments are carried out on lithium-ion batteries. When the battery was in the pulse discharge stage, the current direction of the improved model is shown in  $I_b$ . As the current direction is taken as positive, the Kirchhoff voltage law and Kirchhoff current law equations are listed according to the reference direction of voltage and current as shown in Eq.(13).

$$\begin{cases} U_L = U_{OC}(SOC) - i(t)R_o - U_s - U_L \\ \frac{dU_s}{dt} = \frac{i(t)}{C_s} - \frac{U_s}{R_s C_s}, \frac{dU_L}{dt} = \frac{i(t)}{C_L} - \frac{U_L}{R_L C_L} \end{cases} \quad (13)$$

$U_s$  is the terminal voltage of the parallel circuit composed of  $R_s$  and  $C_s$ .  $U_L$  is the terminal voltage of the parallel circuit composed of  $R_L$  and  $C_L$ . According to the current curve and voltage curve of HPPC constant-current pulse, the battery is in constant discharge for 10 s during  $t_1 \sim t_3$ , and the rest of the time is in the static state. Wherein,  $t_1$ ,  $t_2$ , and  $t_3$  are discharging start time, discharge stop time, and static stop time respectively. By time domain analysis of these two resistance-capacitance circuits in series, the terminal voltage of the resistance-capacitance network in parallel can be obtained as shown in Eq.(14).

$$U_s = \begin{cases} R_s i(t) \left[ 1 - e^{-\frac{(t-t_1)}{\tau_s}} \right] \\ U_s(t_2) e^{-\frac{(t-t_2)}{\tau_s}}, t_2 < t < t_3 \end{cases}, U_L = \begin{cases} R_L i(t) \left[ 1 - e^{-\frac{(t-t_1)}{\tau_L}} \right] \\ U_L(t_2) e^{-\frac{(t-t_2)}{\tau_L}}, t_2 < t < t_3 \end{cases}, t_1 < t < t_2 \quad (14)$$

$\tau_s$  is the time constant of the parallel connection circuit of  $R_s$  and  $C_s$ .  $\tau_L$  for  $R_L$  and the time constant of the parallel connection circuit of  $C_L$ .

## 2.2. Collaborative power state estimation

Accurate lithium-ion battery power state estimation plays an important role in its real-time working state monitoring and safety control. To solve the difficult real-time estimation problem of the

lithium-ion batteries under various operating conditions and low estimation accuracy, the lithium cobalt oxide batteries are taken as the research objects, the working characteristics of which are analyzed comprehensively under various operating conditions. On this basis, the equivalent circuit model is established by considering the importance of early power state estimation accuracy for later iterate calculation. The initial value is calibrated by using the relationship between the open circuit voltage and state of charge, and then the AC-UKF calculation treatment is used for the power state estimation and output voltage tracking, to realize the real-time high-precision power state estimation of lithium-ion batteries, the calculation process of which is shown in

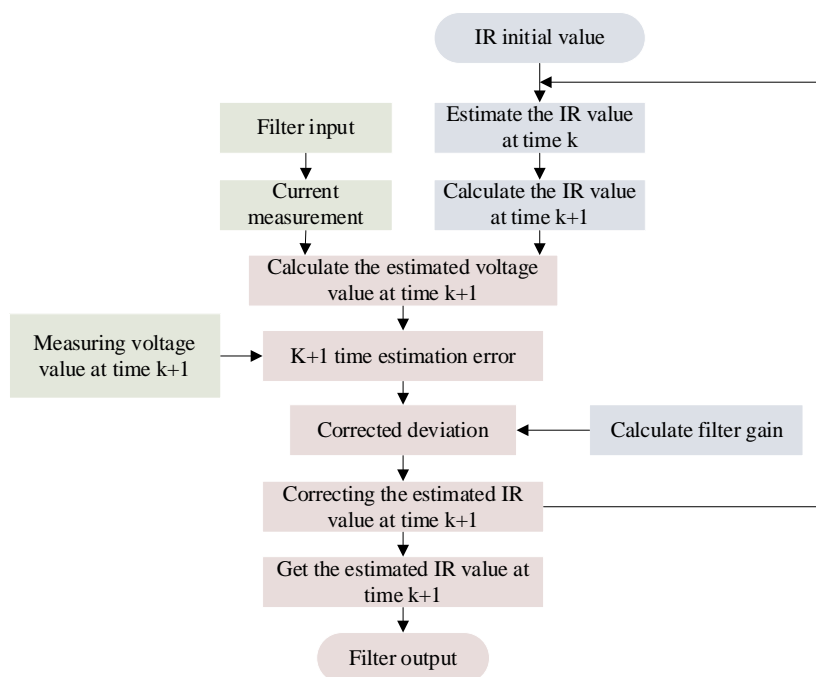


Figure 3. Collaborative power state estimation flow chart

As the dynamic lithium-ion battery working characteristic is typically nonlinear, the equivalent circuit model can simulate the transient response process with high accuracy. It is suitable for high current, step, and complex charge-discharge conditions, according to which the improved circuit model structure is designed. The capacitor  $C_b$  is used to represent the change of open circuit voltage (open circuit voltage) caused by current accumulation.  $E$  is an ideal voltage source, which is used to form a whole to represent the change of open circuit voltage  $U_{OC}$  together with  $C_b$ .  $R_o$  is the internal resistance of the battery, and its terminal voltage is used to represent the instantaneous voltage drop caused by the battery current.  $R_s$  and  $C_s$  are the polarization resistance and polarization capacitance of the battery respectively. They are in parallel to simulate the polarization characteristic process of battery charge and discharge.  $I$  is the loop current of the battery that takes the discharge direction as positive and  $U_L$  is the battery terminal voltage. The experimental model is built in MATLAB/Simulink and its performance analysis is carried out for various working conditions. The experimental results show that the proposed

estimation model can estimate the power state of lithium-ion batteries well with the advantages of fast convergence and good tracking effect, and its estimation error is within 4%, verifying that the AC-UKF algorithm has high accuracy in the power state estimation of lithium-ion batteries. Based on an analysis of this adaptive equivalent model, the calculated expression can be acquired as shown in Eq.(15).

$$\begin{cases} E(t) = U(t) + U_c(t) + R_1 \times I(t) \\ U(t) = \frac{I(t)}{C} - \frac{U_c(t)}{R_2 C} \end{cases} \quad (15)$$

Wherein,  $E(t)$  is the electromotive force of the power supply process, and the relationship between  $E(t)$  and power state is expressed as  $E(t) = f[S(t)]$ . Accurate power state estimation is very difficult. Aiming to realize the internal resistance estimation, there are many common methods. And then,  $S(t)$  can be obtained by combining the ampere hour integral method as shown in Eq.(16).

$$S(t) = S(t_0) - \int_0^t \frac{\eta I(t)}{Q} dt \quad (16)$$

The power state is selected as the system state quantity, the terminal voltage  $U(t)$  as the observation quantity, and  $I(t)$  as the system input quantity. Wherein,  $P$  is the mean square error and  $K$  is the Kalman gain.  $I$  is an  $n \times m$  unit array.  $Q$  and  $R$  are the variances of  $w$  and  $v$  respectively, which do not change along with the system generally. The initial value of the filter and the filter variance are  $X(0) = E[X(0)]$  and  $P(0) = \text{var}[X(0)]$  respectively. The filtering step in the  $(k+1)$  period is described as follows. Firstly, the state of the current time and the mean square error are estimated by using the state parameter  $X_k$  at  $k$  time and the mean square error ( $P_k$ ) to obtain a prior state  $X_{k+1}$  and the prior mean squared error  $P_{k+1}$ , and then the Kalman gain  $K_{k+1}$  at the current moment can be calculated. Finally, the state of the current time  $X_{k+1}$  is obtained by correcting the prior state with  $K_{k+1}$ , and the mean squared error of the current time is obtained by correcting the a priori mean square error parameter  $P_{k+1}$ [58]. However, since this is a discrete system, the relationship between  $S(k+1)$  and  $S(k)$  after discretization is obtained as shown in Eq.(17).

$$S(k+1) = S(k) - \frac{\Delta T}{Q} I(k) + V(k) \quad (17)$$

The system state equation of  $S(k+1)$  and  $S(k)$  represent the  $k+1$  and  $k$  time-point power state values.  $Q$  is the capacity of lithium-ion batteries.  $\Delta T$  is per unit time which is also known as sampling time.  $I(k)$  is the current size and  $V(k)$  is used for its noise influence. The nonlinear transform is an important part of the power state estimation process and its basic idea is to select a limited number of sampling points according to a certain sampling method combined with the statistical characteristics of state variables. What is more, these points need to meet the condition that their mean and covariance are the same as that of the original state, which is then substituted into the nonlinear function to obtain the corresponding set of value points of the nonlinear function. And then, the system measurement equation is obtained as shown in Eq.(18).

$$V(k) = f\{S(k)\} - R_o \times I(k) - U_c(k) + V(k) \quad (18)$$

In the above equation,  $U(k)$  is the electromotive force of the power supply at time moment  $k$ .  $f(S(k))$  represents the nonlinear relationship between the output voltage and its power state.  $R_o$  is the ohm resistance and  $I(k)$  is the current measured at the time point  $k$ .  $U_c(k)$  is the open circuit voltage value at

time moment  $k$ , and  $V(k)$  is its noise influence. Aiming at the nonlinear problems of lithium-ion batteries, the forced linearization of the system is not adopted in the iterate calculation process. The unscented transform is taken as the basis and used to adopt the appropriate sampling strategy to approximate the probability density of the system state variables to obtain the optimal solution. The mean and covariance of the transformation are obtained through these set of points. Therefore, the key to nonlinear transformation lies in the acquisition of sampling points and the determination of their corresponding weights. The dimension of state variable  $x$  is set to be  $n$ . The parameters of  $x$  and  $P$  can be used to describe its mean and covariance matrix respectively, and  $y$  is set to be its observation variable. As a result, the sampling data points  $(2n+1)$  are obtained in this nonlinear system as shown in Eq.(19).

$$\begin{cases} x^i = x, i = 0 \\ x^i = x + (\sqrt{(n + \lambda)P})i, i = 1 + n \\ x^i = x - (\sqrt{(n + \lambda)P})i, i = n + 1 \sim 2n \end{cases} \quad (19)$$

As this prediction method is one of the most widely used intelligent algorithms, it can be introduced into the practical scenarios of the power state estimation of power lithium-ion batteries. The basic principle of the algorithm is to use the minimum mean square error as the optimal estimation criterion, and the state space signal- noise model is used to describe the relationship between the state variables and observed factors by establishing the state and observation equations of the model. The battery charge-discharge current is taken as the system input factors and the terminal voltage is used as the output, according to which the system state is updated continuously by the error correction of the observed terminal voltage value and the estimated battery voltage value, thereby obtaining the minimum-variance estimated power state value. The corresponding weights are shown in Eq. (20).

$$\begin{cases} \omega_m^0 = \lambda / (n + \lambda) \\ \omega_c^0 = \lambda / (n + \lambda) + (1 - \alpha^2 + \beta) \\ \omega_m^i = \omega_c^i = \lambda / 2(n + \lambda) \end{cases} \quad (20)$$

In the formula,  $\alpha$  and  $\beta$  are auxiliary scale factors, which are also used as the scaling parameters. The estimation process of the Kalman filter algorithm includes time update and measurement update steps. The time update step is also called the prediction process, which is a one-step prediction of the current state variable and provides the priory estimation process for the next time moment. The measurement update step is also called the calibration process, which is a feeding back process of the observations aiming to correct the deviations. The nonlinear transfer of these sampling points together with its mean and covariance value after the transformation calculated as shown in Eq.(21).

$$\begin{cases} y^i = f(x_i), \hat{y} = \sum_{i=0}^{2n} \omega_i f(x_i), i = 0 \sim 2n \\ P_y = \sum_{i=0}^{2n} \omega_i [f(x_i) - \hat{y}][f(x_i) - \hat{y}]^T \end{cases} \quad (21)$$

Combined with the adaptive equivalent circuit model and considering the practical application, only state of charge parameter  $S$  is selected as the system state variable, and the terminal voltage  $U$  of the battery is taken as the observation variable. The state space expression of the established battery model is shown in Eq.(22).

$$\begin{cases} S_{k+1} = S_k - I_k \Delta t / (Q_N) + \omega_k \\ U_{0,k+1} = f(S_{k+1}) - U_R - U_1 + v_{k+1} \end{cases} \quad (22)$$

Wherein, the power state value at time point  $k$  is predicted at time point  $k+1$ .  $\Delta t$  is the sampling interval time.  $Q_N$  is battery rated capacity and the capacity calibration is actually required.  $I_k$  is the current at time point  $k$ , the charging direction of which is set as positive.  $f(S_{k+1})$  is the relationship between battery open circuit voltage and its power state.  $\omega$  and  $v$  are the process noise and observation noise respectively. These Sigma points are transferred through the system state equation, and the predicted value point group can be obtained consequently. Then, through the Kalman gain and the error between the real value of the observed variable and the prediction, the predicted value is modified constantly and the optimal estimation value of the system state variable is obtained finally. The power state variable value at time point  $k$  can be set together with its error variance matrix  $P_k$ . The specific process is described as follows. As can be designed in the prediction stage, the expected value of the system state variable at time point  $k+1$  is shown in Eq.(23).

$$\begin{cases} x_{k+1|k}^i = f(x_k^i, u_k) \\ \hat{x}_{k+1|k} = \sum_{i=0}^{2n} \omega_m^i x_{k+1|k}^i \end{cases} \quad (23)$$

Wherein,  $u_k$  is the input variable. One-step prediction of sampling points is then made by the combined equations. After weighted sum treatment, the predicted mean value of system state quantity is obtained. The state and observation equations are used to make the best estimation of the minimum variance of the state through the observation value of the system input and output parameters. Its implementation process can also be divided into two stages of prediction and update. The sampling Sigma points are selected according to the symmetric sampling strategy in conditions that the sigma points need to meet, which have the same mean and covariance values with the original state. Similarly, the error variance matrix at time  $k+1$  is predicted as shown in Eq.(24).

$$P_{x,k+1|k} = \sum_{i=0}^{2n} \omega_c^i [x_{k+1|k}^i - x_{k+1|k}] [x_{k+1|k}^i - x_{k+1|k}]^T + Q_{k+1} \quad (24)$$

As a result, the Sigma sampling points are updated subsequently, according to which the sampling data points are obtained and updated in combination with the calculation equations. The one-step prediction value at the time moment  $k+1$  of each sampling point is put into the system observation equation, aiming to acquire the predicted value of each sampling data point. Consequently, the weighted mean value of measurement parameters at the time moment  $k+1$  is shown in Eq.(25).

$$\begin{cases} y_{k+1|k}^i = h(x_{k+1|k}^i, u_{k+1}) \\ \hat{y}_{k+1|k} = \sum_{i=0}^{2n} \omega_m^i y_{k+1|k}^i \end{cases} \quad (25)$$

The real-time observation and correction should be conducted for the state variable estimation, in which the Kalman filtering is conducted to estimate the essential state of the lithium-ion batteries together with the ampere-time integration treatment, in which the measured voltage value is used to correct the real-time predicted. When estimating the battery power state by using the Kalman filtering algorithm, it is necessary to establish a suitable iterate calculation model structure and the estimation accuracy largely depends on the accuracy of the battery model. When the Kalman filtering method is

used to estimate the battery power state value, it should be regarded as a power supply system and the internal resistance is one of its state parameters. The variance matrix of measured values and the covariance between state quantity and measurement at time point  $k+1$  are calculated as shown in Eq.(26).

$$\begin{cases} P_{yy,k+1} = \sum_{i=0}^{2n} \omega_c^i [y_{k+1|k}^i - \hat{y}_{k+1|k}] [y_{k+1|k}^i - \hat{y}_{k+1|k}]^T + R_{k+1} \\ P_{xy,k+1} = \sum_{i=0}^{2n} \omega_c^i [x_{k+1|k}^i - \hat{x}_{k+1|k}] [y_{k+1|k}^i - \hat{y}_{k+1|k}]^T \end{cases} \quad (26)$$

Subsequently, the high-precision power state estimation methods include neural network, fuzzy reasoning, and Kalman filtering algorithms. As the Kalman filtering method is an optimized autoregressive data processing algorithm, the internal resistance estimation accuracy can be improved by its real-time optimal estimation of the state variables and its extended application performs the first-order linearization on Taylor expansion of these nonlinear functions. In the update stage, The Kalman gain is calculated as shown in Eq.(27).

$$K_{k+1} = P_{xy,k+1} / P_{yy,k+1} \quad (27)$$

To better reflect the dynamic characteristics of ternary dynamic lithium-ion batteries in the step of charging and discharging conditions, the polarization circuit of the model is extended and an improved model is obtained. The model uses a double resistance-capacitance circuit instead of the single resistance-capacitance circuit. Where, the parallel circuit composed of  $R_s$  and  $C_s$  has a small time constant, which is used to simulate the rapid change of voltage in the case of current mutation. The parallel circuit composed of  $R_L$  and  $C_L$  has a large time constant, which is used to simulate the slow and stable voltage process. The improved circuit model can characterize the polarization characteristics of the battery and simulate the static circuit. The updated system state variable value and the error variance matrix are updated as shown is shown in Eq.(28).

$$\begin{cases} \hat{x}_{k+1|k+1} = \hat{x}_{k+1|k} + K_{k+1} (y_{k+1} - \hat{y}_{k+1|k}) \\ P_{x,k+1|k+1} = P_{x,k+1|k} - K_{k+1} P_{xy,k+1} K_{k+1}^T \end{cases} \quad (28)$$

According to the power state estimation model for lithium-ion batteries, the programming schedule is established in MATLAB/Simulink, which is then verified by combining with various experimental data. As for each component module of the experimental model, various parameters and weights of the algorithm are determined in its sub-module to prepare for Sigma points of its power state quantity. Subsequently, the Sigma points are obtained in the module according to the symmetric sampling strategy which is identical with the original state mean and covariance. In the power state estimation sub-module, the obtained Sigma points are transferred nonlinear once, and the weighted sum treatment is used to calculate the predicted mean value of the state quantity at the next time point. The sigma points are then updated by the predicted mean value and transformation module. The updated Sigma points predict the observed quantity according to the observation equations by using the Kalman gain that is calculated in advance and the correction parameters are obtained subsequently. In the state variable and error update modules, the predicted mean value and its corresponding error covariance are updated according to the real-time observation data and Kalman gain until the next iteration is complete. In order to verify the effectiveness of the proposed algorithm based on an adaptive equivalent model, the relationship between power electromotive force and power state is calculated by introducing the

experimental data of aviation lithium-ion batteries. The framework of the iterate calculation system is constructed as shown in Figure 4.

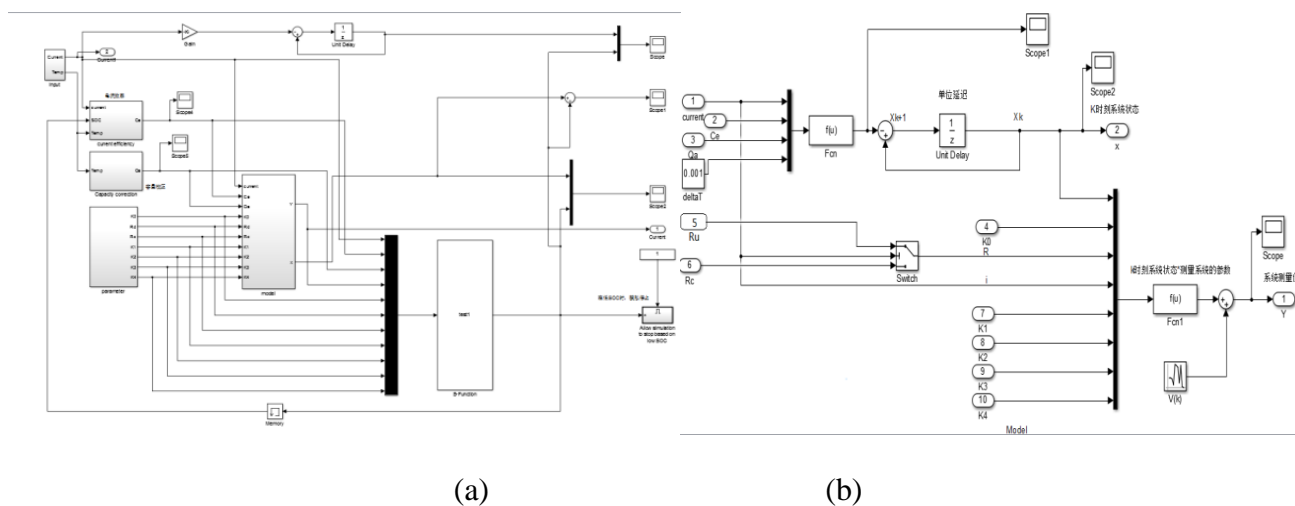


Figure 4. Iterate calculation system block diagram

The figure above is the block diagram of the iterate calculation system by considering the battery model structure that is obtained for the aviation lithium-ion battery, which describes the process of the AC-UKF algorithm.

### 3. EXPERIMENTAL ANALYSIS

#### 3.1. Equipment and procedures

This experiment takes lithium cobalt oxide battery with parameters of 3.70 V and 70 Ah as the research object, and the experimental results are analyzed comprehensively combined with its working characteristics and principles. The internal resistance of lithium batteries has always been an important indicator of lithium batteries. The characteristics of the internal resistance of ternary lithium batteries are studied by taking the ternary lithium battery as the research object, in which the HPPC test method is introduced to test the internal resistance under different pulse currents and pulse durations during the charge and discharge conditions[59]. The experimental temperature is 25 °C, and the law of internal resistance changes under charge and discharge conditions is obtained, in which the internal time-varying resistance shows a decreasing trend along with the power state increase. The internal resistance of the discharge process is higher than the internal resistance of the charging process and the internal resistance of the discharge process tends to be stable after  $S = 0.3$ . As the pulse time increases, the internal resistance increases as well and the internal resistance at  $S = 0.1$  and  $S = 0.2$  is significantly higher than the internal resistance when  $S$  changes from 0.3 to 0.9. The basic technical parameters of the experimental lithium-ion batteries are shown in Table 1.

**Table 1.** Basic technical parameters of the battery

Factor	parameter
Size: length * width * height /mm	200*80*180
Rated voltage/V	3.70
Maximum load current /A	1.5C
Charge cut-off voltage/V	4.15
Discharge cutoff voltage/V	3.0
Working temperature /°C	-15~70
Rated capacity/Ah	70.0

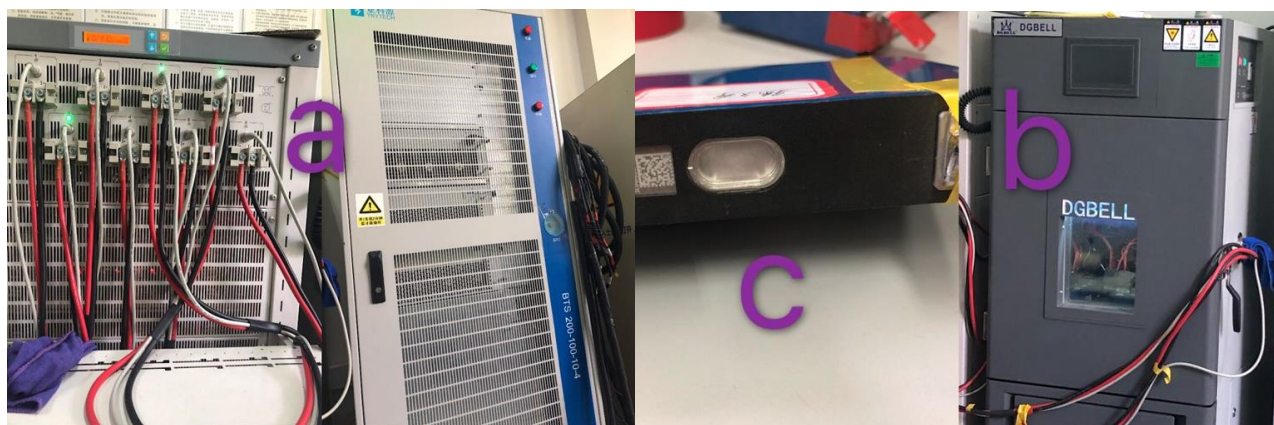


**Figure 5.** Experimental platform

The battery HPPC experimental charging and discharging equipment is the power battery large-rate charge and discharge tester (CT-4016-5V100A-NTFA) made by Shenzhen Xinwei New Energy Technology Co., Ltd. The incubator is a three-layer independent temperature control high and low temperature test chamber (DGBELL BTT-331C) of Dongguan Bell Experimental Equipment Co., Ltd., and the experiment was carried out at a constant temperature of 25 °C, the experimental platform is shown in Figure 5.

As expressed in Figure 5, several parts can be known from the experimental platform. Part a is the experimental facility for the charging and discharging test, the equipment code is BTS 750-200-100-4. The high energy lithium-ion batteries are shown in Part c, which is settled into the content temperature equipment as shown in Part b.

### 3.2. Identification experiments

The parameter measurement process should have little damage to the battery [60], which is used to measure its internal resistance and other factors that are influencing the working characteristics of the power lithium-ion batteries. This experiment requires the measurement of transient internal resistance, according to which the test method itself has little effect on the internal resistance variation, which provides the internal resistance value by applying time-varying current to the battery. Applying current

into the instantaneous internal resistance the experimental HPPC test method is introduced for the parameter identification, the parameter identification steps of which are described as follows. Firstly, the lithium cobalt oxide batteries are subjected to the cyclic charge-discharge process, in which the batteries are charged and discharged three times. The charging rate is set as 0.2 C that continues until its terminal voltage reaches 4.15 V, and then it is discharged at 0.1 C current rate to the cutoff voltage of 3.0 V. As a result, the lithium-ion batteries are activated after being fully charged and fully discharged for 12 hours. Secondly, the lithium cobalt oxide battery is charged fully with its power state equaling to 1, which is discharged at a rate of 1 C for 3 minutes ( $S=0.95$ ) and left for 40 minutes subsequently. Afterward, the HPPC experiments are performed, and the open circuit voltage and the discharge current are recorded along with the discharge time expansion. And then, the second step is repeated by discharging 5% capacity per cycle, and the HPPC experiments are performed at different power state values as 0.9, 0.85, 0.8, ..., and 0.05 respectively. According to the HPPC experimental data of each state of charge test point, the parameter values in the circuit model can be obtained corresponding to different power state levels as shown in Tab. 2. The experimental SOC interval of reference [59] is 0.1, and the SOC interval of this experiment is 0.5.

As can be known from Tab. 2, the ohm internal resistance  $R_o$  increases slowly with the power state decrease, in which the variation range is small and the change rate is slow. The polarization internal resistance  $R_p$  decreases slowly along with the power state decrease, which increases sharply when the power state is lower than 0.15 along with the acceleration increasement. After being left for a long time, the effects of polarization and ohm internal resistance are greatly reduced. At this time point, the measured battery terminal voltage is the open circuit voltage, that is, the battery electromotive force  $E$ . The voltage of the lithium-ion battery terminal drops rapidly from the stage  $S=1.00$  to  $S=0.85$ , and the open circuit voltage decreases by 0.04 ~0.06 V for every power state decrease of 0.05. When the power state enters a stable period between 0.85 and 0.15, the open circuit voltage drop is basically stable within 0.03 V for every power state decrease of 0.05 and the voltage fluctuation is small. After the power state is lower than 0.15, the open circuit voltage drops very rapidly and the voltage fluctuates greatly along with the battery discharging process. The experimental results show that when the power state is lower than 0.15, that is, after the lithium-ion battery is deeply discharged, the internal chemical reaction of the battery is severe and the competitions vary drastically.

**Table 2.** Model parameters under different power states

SOC	$R_o/m\Omega$	$R_p/m\Omega$	$C_p/KF$	OCV/V
1.00	6.0661	6.9821	0.2041	4.13
0.95	6.1911	6.7857	0.2101	4.09
0.90	5.9214	6.8321	0.2090	4.05
0.85	5.8625	6.3768	0.2216	3.99
0.80	5.8214	6.2018	0.2166	3.96
0.75	6.0839	6.1911	0.2320	3.92
0.70	6.0196	6.0000	0.2391	3.89
0.65	6.0589	6.0786	0.2333	3.86
0.60	6.0321	6.0679	0.2465	3.84

0.55	6.3286	6.0857	0.2336	3.82
0.50	6.7232	6.0714	0.2347	3.81
0.45	6.8643	6.1893	0.2315	3.79
0.40	7.2929	6.0571	0.2358	3.78
0.35	7.0500	6.2268	0.2313	3.76
0.30	7.8054	6.6268	0.2162	3.74
0.25	8.0339	6.5214	0.2217	3.72
0.20	8.0161	6.7714	0.2114	3.70
0.15	8.2464	6.8786	0.2072	3.69
0.10	7.8679	8.4786	0.1692	3.58
0.50	8.5714	18.5536	0.0766	3.28

**Table 3.** Internal resistance under different conditions of the charging process

charge SOC	Pulse current2C			Pulse current3C			Pulse current4C		
	10sR	20sR	30sR	10sR	20sR	30sR	10sR	20sR	30sR
0.1	51.13	56.67	59.62	45.82	49.73	52.77	39.80	43.80	46.32
0.2	41.35	46.17	51.78	40.35	45.48	48.71	36.21	41.51	44.81
0.3	40.25	45.04	48.14	38.42	43.93	46.39	33.71	38.28	41.33
0.4	39.81	44.60	47.00	37.40	41.60	43.93	32.51	37.30	39.80
0.5	37.64	41.78	44.17	36.25	39.87	42.77	32.84	36.97	38.83
0.6	37.21	41.56	45.26	35.39	40.60	44.36	31.97	36.69	39.79
0.7	39.16	46.78	49.64	37.70	43.64	46.25	34.04	38.61	41.41
0.8	39.60	44.60	48.74	39.14	42.33	44.95	32.63	37.73	40.67
0.9	38.73	43.90	46.78	37.12	42.33	44.55	33.39	38.28	40.78

**Table 4.** Internal resistance under different conditions of the discharging process

discharge SOC	Pulse current2C			Pulse current3C			Pulse current4C		
	10sR	20sR	30sR	10sR	20sR	30sR	10sR	20sR	30sR
0.1	64.84	74.62	80.07	64.84	71.92	77.84	55.13	66.12	75.14
0.2	44.84	50.19	54.51	44.22	50.89	54.36	42.09	47.96	52.09
0.3	40.03	45.04	48.14	39.87	44.94	48.14	38.50	43.61	46.87
0.4	37.85	42.68	46.77	38.13	42.62	46.69	37.96	40.96	43.50
0.5	38.08	42.43	45.04	36.24	41.17	44.08	36.21	39.80	42.09
0.6	37.64	42.63	43.73	37.84	42.34	43.93	36.45	40.45	42.41
0.7	41.97	46.56	49.39	39.15	43.39	46.98	37.03	41.73	44.69
0.8	41.74	46.56	48.96	39.26	43.78	46.97	39.60	40.89	43.89
0.9	40.49	44.82	47.87	40.89	44.51	46.64	37.61	41.54	44.37

The identification steps are as follows:(1) The ternary lithium battery is put in the temperature control box. Set the temperature to 25°C, the humidity to 30%. Shelve the battery for one hour. Then, charge and discharge with 2.3A. Record charge is C; (2) Constant current discharge at 1C rate. Don't

stop discharging until the discharge capacity is 0.01C. At this time. The SOC of the battery is 0.9. And shelve the battery for one hour. The voltage is recorded as U1; (3) Constant current discharge of the battery using pulse current of XC rate. And last 30 seconds. The voltage is recorded as U2. Then, Shelve the battery for 60 seconds. The voltage is recorded as U3. (4) Constant current charge of the battery using pulse current of XC rate. And last 30 seconds. The voltage is recorded as U4. Then, Shelve the battery for 60 seconds. (5) Repeat steps 2 to 4 until SOC=0.9, (6) Let X=2,3,4. Repeat steps 1 to 5. Perform internal resistance testing of different pulse currents. Reference compensation method for measuring internal resistance. Calculate internal resistance. The internal resistance test results of different pulse currents and different pulse times corresponding to the charge and discharge process.

The internal resistance changes under different pulse durations during charge and discharge with a pulse current of 3C. The internal resistance increases with the increase of the pulse time, and the amplitude of the increase gradually decreases Under the same SOC. For example, when SOC=0.5, the internal resistance of the pulse time is 10s 20s and 30s respectively is 36.25, 39.87, and 42.77.mΩ. That is, for every 10s increase in pulse length, the internal resistance increases from 3.6 to 2.9mΩ. In addition, the internal resistance changes with the SOC in the overall trend as the length of the pulse increases. It slowly decreases and then slowly rises and finally stabilize as shown below separately.

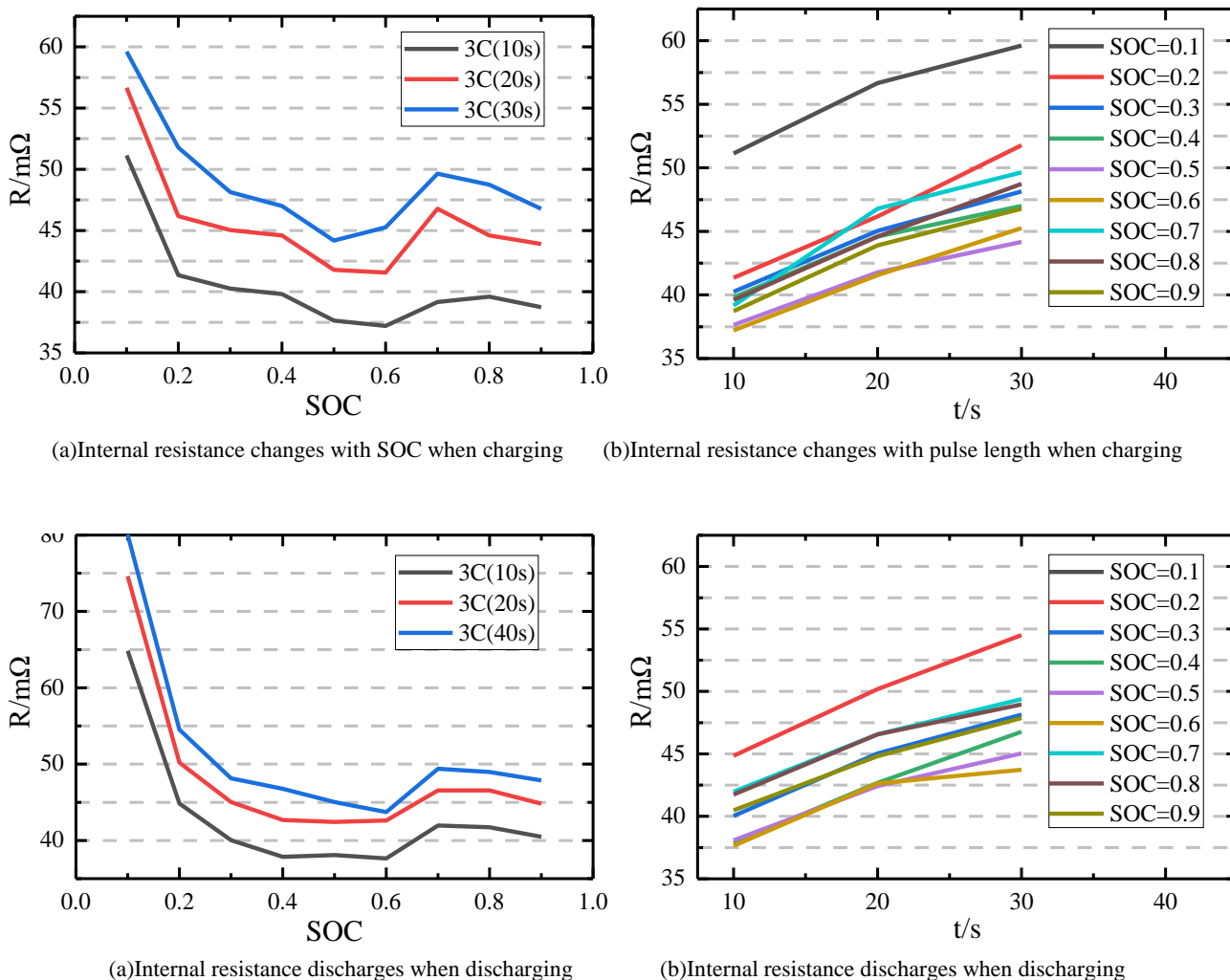
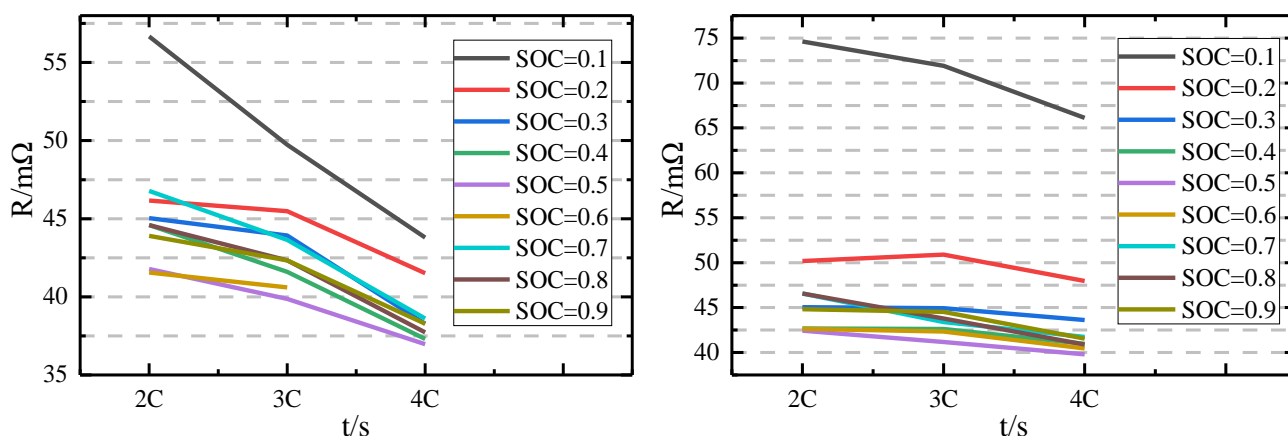


**Figure 6.** Change of internal resistance during discharging when the pulse current is 3C

The internal resistance changes under different pulse durations during discharge with a pulse current of 3C. Internal resistance increases at discharge progress as the pulse time increases. Unlike the charging process, the internal resistance decreases rapidly when SOC=0.1 and SOC=0.2 during discharge. The internal resistance tends to be stable between SOC=0.3 and 0.9, and the range of variation is small. The internal resistance is basically stable at 38.77 at 10s pulse time between SOC=0.3 and 0.9. The internal resistance is basically stable at 43.33 at 20s pulse time between SOC=0.3 and 0.9. The internal resistance is basically stable at 46.30 at 30s pulse time between SOC=0.3 and 0.9. Before SOC=0.3, the internal resistance is higher under different pulse lengths. The maximum internal resistance at 10s reaches 64.81mΩ. The maximum internal resistance at the 20s reaches 71.92mΩ. The maximum internal resistance at the 30s reaches 77.86mΩ.

The variation of internal resistance with pulse current during charge and discharge at the same SOC for current pulse multipliers of 2C, 3C, and 4C. As can be seen from the figure: The internal resistance is close to decreasing linearly as the pulse current increases. SOC=0.3 to 0.9 change trend consistent. And with the pulse current, the difference in internal resistance corresponding to different SOC values is not large. Under different pulse currents, the internal resistance difference between the charging process SOC=0.1 and SOC=0.2 is 9.78mΩ. the internal resistance difference between the discharging process SOC=0.1 and SOC=0.2 is 20.02mΩ. During the charging and discharging process, the internal resistance at different pulse currents at SOC=0.1 is significantly higher than the resistance at SOC=0.1 to 0.9. During the charging and discharging process, the internal resistance at different pulse currents at SOC=0.1 is significantly higher than the resistance at SOC=0.1 to 0.9.



(a)charging progress at 20s pulse time

(b)discharging progress at 20s pulses time

**Figure 7.** Change of internal resistance during charge and discharge when pulse current is 2C, 3C, 4C

The ternary lithium battery is taken as the research object. The relationship between internal resistance and SOC, pulse time, pulse current and charge and discharge state is studied with reference to HPPC mixed pulse power characteristic test. And the influence of current size on the test is analyzed. Firstly, the internal resistance at SOC=0.1 is higher than the internal resistance of SOC=0.2 to 0.9 under the different pulse lengths regardless of the charging process or the discharging process. Secondly, under different pulse lengths, the internal resistance during discharge will be higher than the internal resistance

during charging. Finally, During the charging and discharging process, as the pulse current increases, the internal resistance can be approximately considered to decrease linearly.

### 3.3. Constant current effect

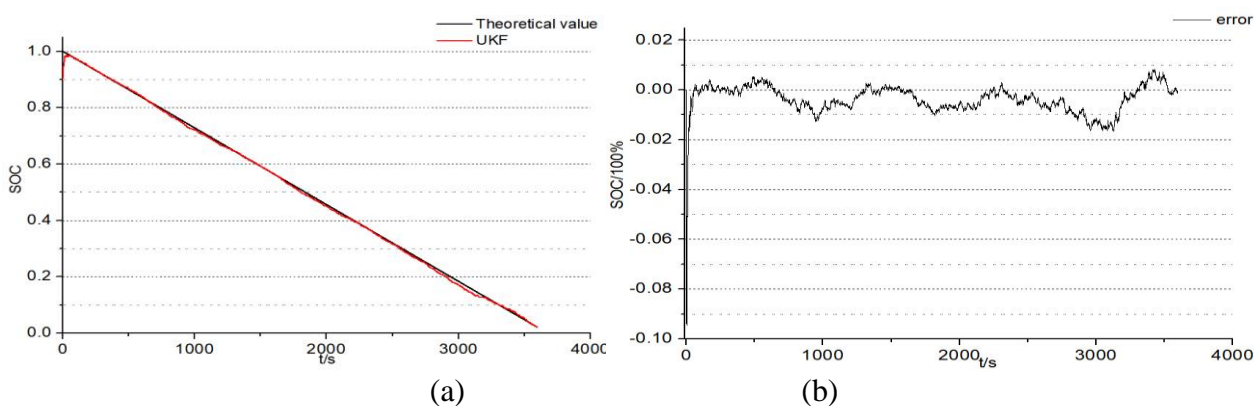


**Figure 8.** Power state estimation under constant current discharge conditions

The experimental analysis is conducted in MATLAB/Simulink according to the power state estimation model of lithium-ion batteries that is established above, in which the verification schedule is carried out under both of the constant and time-varying discharging current conditions. Subsequently, the lithium-ion battery is discharged completely by using the constant 1 C discharge current rate. The experimental results are shown in Figure 8.

The initial power state value of the experimental test is set to be 0.9, which is different from the theoretical value of 1.0 to verify its convergence effect in the real-time iterate calculation process. As can be known from the experimental results, the comparison curve between theoretical power state estimation and the proposed iterate calculation algorithm has good tracking results. Although the initial power state value is different from the theoretical value, it can track the real power state value quickly with good estimation stability, the calculated error of which decreases rapidly stable within  $\pm 2.00\%$  compared with the real value, proving that the proposed power state estimation approach is of high accuracy. It is worth noting that the power state estimation error becomes larger when the battery is at the end of discharge, and the huge error is mainly caused by the nonlinearity of the battery itself as the nonlinearity of the battery is very strong at the end of power state period. What is more, the maximum error of power state estimation at the end of discharge time point is also within 2.00%.

### 3.4. Cyclic discharging analysis

The experimental results can be obtained by the tests, according to which the state of charge value obtained by the proposed algorithm is very close to the real-time varying power state value, realizing the prediction effectively. Considering the intermittent discharge state of the lithium-ion battery in the practical application, the model is further simulated and analyzed under the experimental cyclic

discharge shelving conditions. The relationship between the open circuit voltage and state of charge is obtained by the experiment as shown in Figure 9.

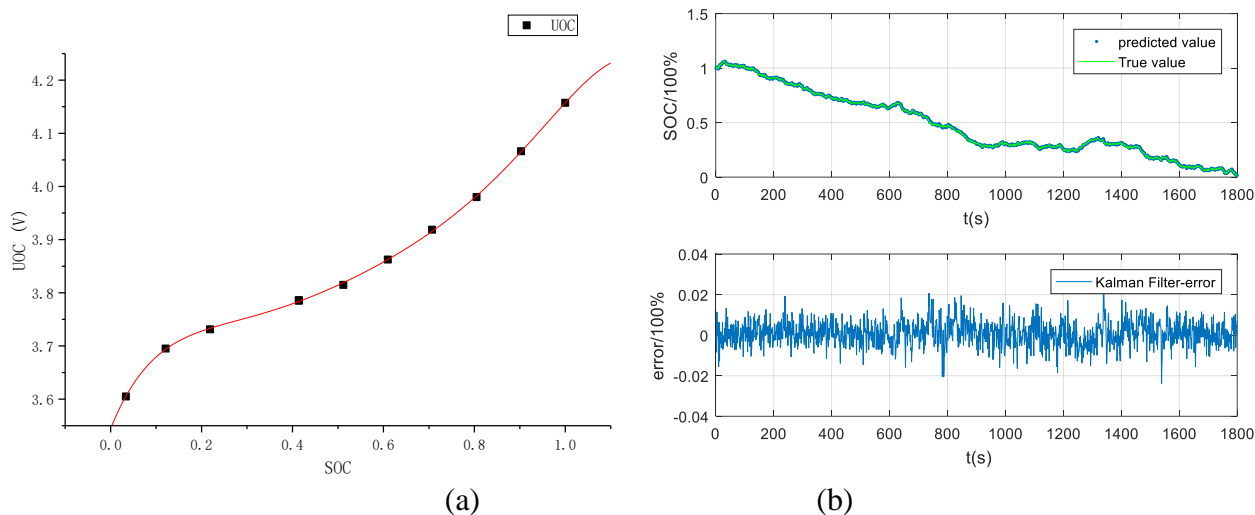


**Figure 9.** Open circuit voltage-power state relationship and the estimation result

Real-time current and voltage data can be acquired under the experimental early cyclic discharging conditions which is then imported into the modeling process. Wherein, the discharge current was 1 C multiplier and the battery will be shelved for 30 mins after every 6-min discharge treatment. The theoretical calculation can be realized for the battery power state estimation by the correction strategies, in which the initial estimated value is set to be 0.5. As can be seen from the experimental results, the proposed algorithm has good convergence and tracking effect, in which the initial algorithm converges rapidly and the required time is about 120 s to track the theoretical value. Subsequently, the discharge cycle is continued until the battery is discharged to the cut-off voltage level, the experimental results of which are shown in Figure 10.

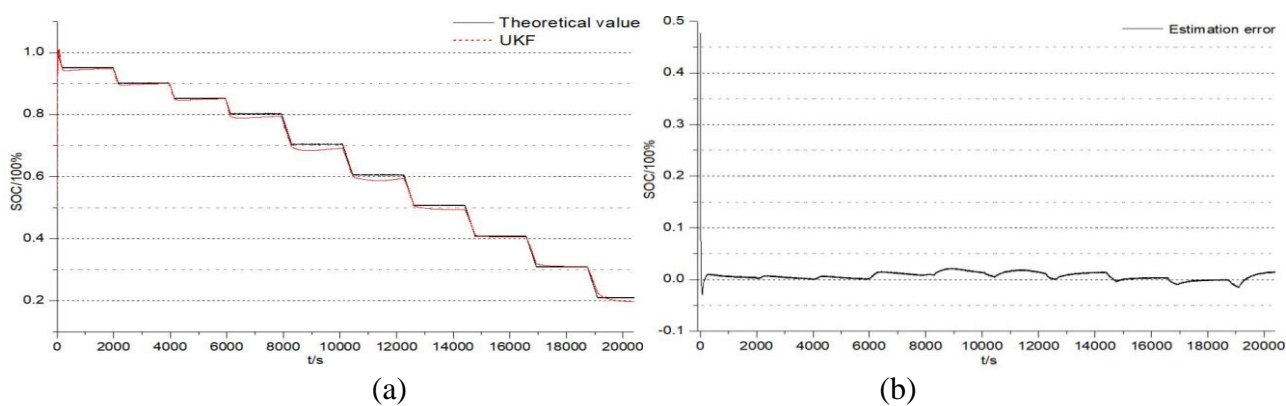


**Figure 10.** Cyclic discharge power state estimation

The estimated deviation is stable within 2.00% and the overall performance is excellent, which proves that it has good convergence and traceability for power state estimation. It is worth noting that the power state estimation error is large than normal when the battery is in the suspended state. This is because the battery equivalent circuit model is hysteresis in a suspended state with deviation and need more time to get the real-time accurate voltage of the battery, which suggests that the adaptive equivalent circuit model can conduct effective correction for the battery performance characterization when there are some deficiencies.

### 3.4. Dynamic test conditions

In practical applications, the real-time current of lithium-ion batteries should be complex and variable. In different working conditions, it is often accompanied by sudden switching and stopping of current and it puts forward strict requirements on the dynamic performance of the battery and brings difficulties to the power state estimation of the lithium-ion batteries in complex working conditions. To further verify the complex application conditions, the response of the model to the charged state of lithium-ion battery is estimated and the customized experimental data are used for its experimental verification. Under the same working conditions, the traditional ampere hour integral and extended Kalman filtering algorithms are added for its synchronous experimental analysis to compare and analyze the prediction effect of the proposed iterate calculation method.

Specific experimental steps are designed as follows. Firstly, the battery is charged completely by using the constant current - constant voltage treatment, in which the constant current rate is 1 C and the upper limit termination voltage is 4.2 V. And then, it is charged at a constant voltage, the cut-off current rate of which is 0.05 C. Secondly, the battery is shelved after charging to stabilize the battery voltage. Since the selected lithium-ion battery has a small capacity, the standing time is selected as 30 mins. Thirdly, the constant current discharge is investigated with the 0.5 C multiplier by lasting 4 mins, and the battery should be standing for 30 s after stopping the discharge treatment. Fourthly, the lithium-ion battery should be charged by using the constant-voltage-constant-current method by using a 0.5 C multiplier. Along with a duration of 2 mins, the battery is left standing for 30 s after stopping its charging process. The constant banishment is conducted by using the 1 C current ratio with a duration of 4 mins. The whole experiment can be realized by cycling the steps of 3 to 5 until the end limitation of the battery discharge demonstration. Consequently, the experimental voltage and current data can be obtained as shown in Figure 11.

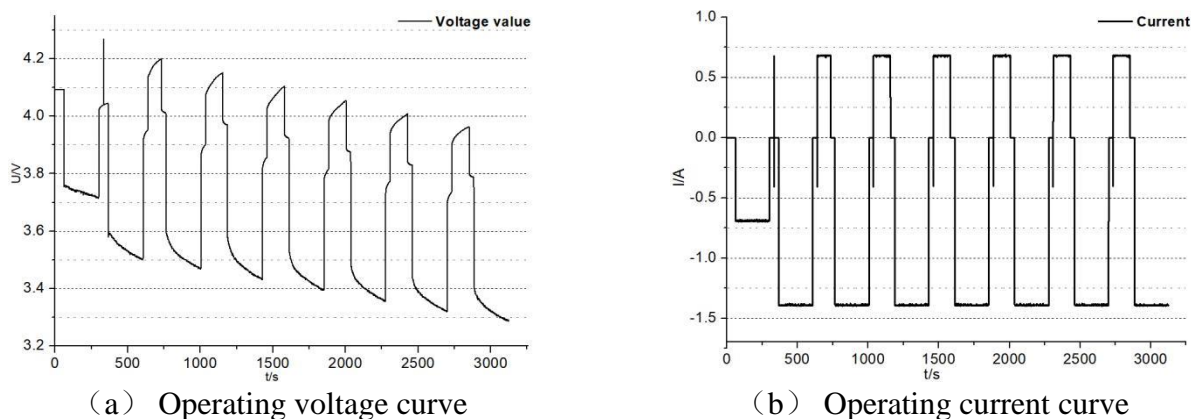


**Figure 11.** Battery voltage and current curve under dynamic working conditions

**Table 5.** Estimation error comparison under complex working condition tests

Algorithm	average error	maximum error	convergence time (s)
Ah	8%	4%	-
EKF	0.2%	0.3%	200
AC-UKF	0.1%	0.1%	4

The voltage and current data obtained from the experiment were imported into the MATLAB platform to analyze the estimation model. The Ah, EKF, and AC-UKF are used respectively to conduct the comparison between the power state values and the theoretical value of the battery, in which the battery starts discharging at full charge and its initial power state is considered to be 1. The overall power state estimation shows a fluctuational downward trend, which is due to the alternating charge-discharge process during the experiment. The initial estimation value of the algorithm is randomly set as 0.95, and the convergence effect of the algorithm in the estimation process and the tracking of the real value have been verified, in which the statistics of experimental data are shown in Tab. 5.

As can be known from the experimental result, the Ah integral method cannot converge rapidly and can only track the real value at the early stage of the estimation process. Moreover, its estimation error is much larger than that of other algorithms. With the extension of estimation time, the error becomes larger and larger. The other two algorithms can track the real power state value and its error is stable in the later estimation as shown in Fig 12.

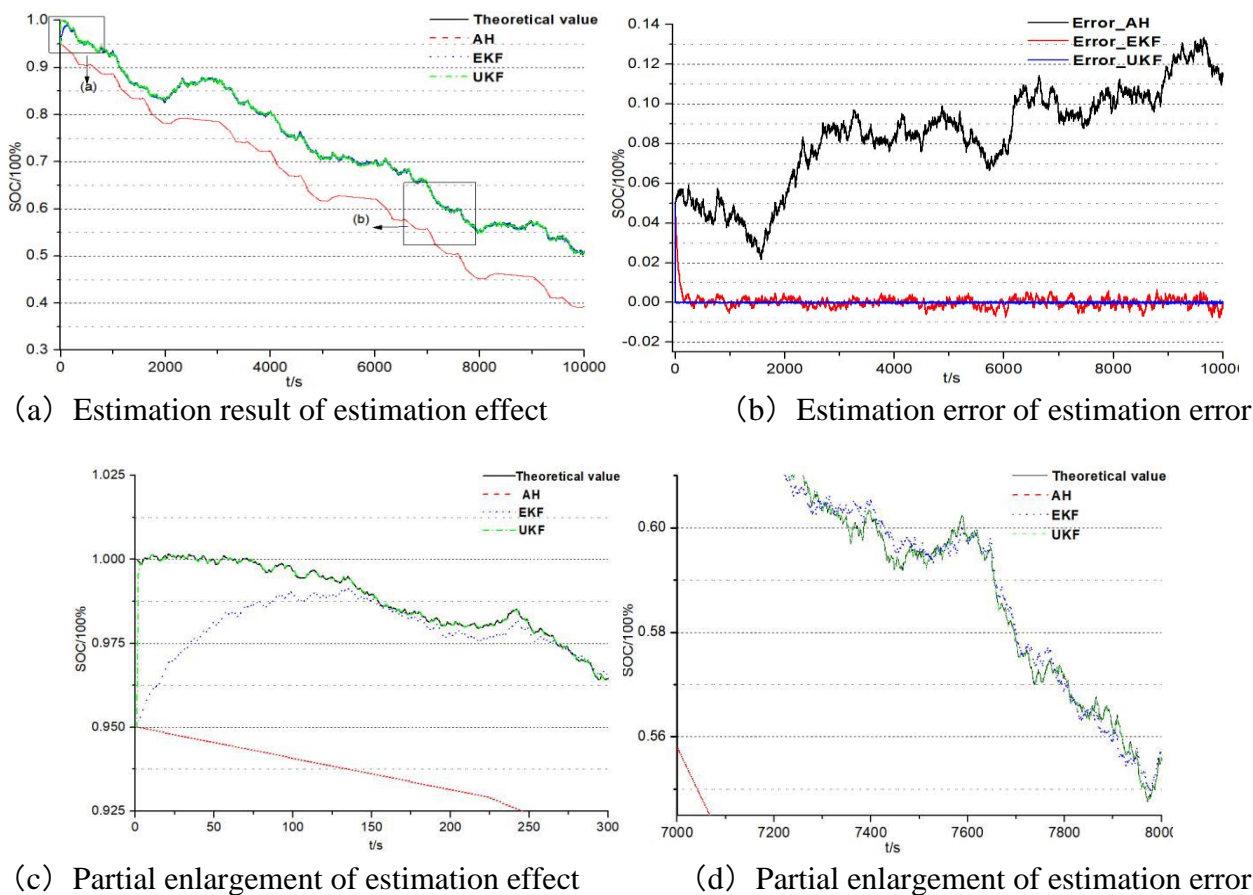


**Figure 12.** Partial enlargement of the estimation effect under complex working conditions

As can be known from the experimental results, the proposed method can converge more rapidly to the real value compared with other traditional algorithms and its estimation error is smaller obviously, the max estimation error of which is 3.87%, verify the superiority of the proposed method in estimating lithium-ion battery power state applications. Based on previous research work, MATLAB/Simulink is used to establish the estimation experimental model and the functions of each component module are analyzed. The model is simulated and analyzed by combining with real experimental data under various operating conditions, such as constant discharge condition, cyclic discharge shelving condition, and complex working conditions, and the feasibility of model estimation is verified by comparison. The results show that the proposed algorithm has fast convergence speed and good tracking effect in estimating lithium-ion battery power state, in which the estimation deviation is stable and the overall performance is excellent. The experimental results show that the established estimation model can better estimate the power state of lithium-ion batteries, with fast convergence speed, good tracking effect, and estimation error, verifying its high accuracy in the power state estimation of lithium-ion batteries.

#### 4. CONCLUSIONS

Accurate power state estimation plays an important role in the real-time working state monitoring and safety control of high energy lithium-ion batteries. In order to solve the difficulty and low accuracy

problems in its real-time power state estimation under various operating conditions, its working characteristics are analyzed comprehensively under various operating conditions. An improved collaborative equivalent model is established to characterize its working characteristics. Considering the importance of the precious estimation accuracy for the later iterate calculation and correction, the initial power state value is calibrated by using the relationship between open circuit voltage and state of charge. And then, an AC-UKF algorithm is put forward and applied for the state of charge estimation and output voltage tracking so as to realize the real-time high-precision lithium-ion battery power state estimation. As can be known from the experimental results, the established model can predict the power state of high energy lithium-ion batteries conveniently with high convergency speed, good output voltage tracking effect, and high accuracy, providing an effective working state monitoring and safety protection method in the cleaner production process of the high energy lithium-ion batteries.

#### ACKNOWLEDGEMENTS

The work was supported by the National Natural Science Foundation of China (No. 61801407) and Natural Science Foundation of Southwest University of Science and Technology(No.17zx71110).

#### References

1. U. R. Farooqui, A. L. Ahmad and N. A. Hamid, *Renew. Sust. Energ. Rev.*, 77 (2017) 1114.
2. D. I. Stroe, M. Swierczynski, S. K. Kaer and R. Teodorescu, *Ieee T Ind Appl.*, 54 (2018) 517.
3. M. Tariq, A. I. Maswood, C. J. Gajanayake and A. K. Gupta, *Ieee Access*, 6 (2018) 41785.
4. R. V. Bhat, M. Motani and T. J. Lim, *Ieee T Wirel Commun.*, 16 (2017) 2822.
5. Z. W. Ni, R. V. Bhat and M. Motani, *Ieee Internet Things*, 5 (2018) 2741.
6. Z. C. Huang, D. F. Chu, C. Z. Wu and Y. He, *Ieee T Intell Transp.*, 20 (2019) 959.
7. D. J. Noelle, M. Wang, A. V. Le, Y. Shi and Y. Qiao, *Appl Energy*, 212 (2018) 796.
8. M. J. Lacey, *Chemelectrochem*, 4 (2017) 1997.
9. J. H. Ahn and B. K. Lee, *Ieee T Power Electr*, 34 (2019) 3041.
10. Z. B. Zhou, M. B. I. Camara and B. Dakyo, *Ieee T Veh Technol.*, 66 (2017) 5775.
11. Z. K. Wang, S. K. Zeng, J. B. Guo and T. C. Qin, *Energy*, 167 (2019) 661.
12. X. Y. Wang, X. Z. Wei and H. F. Dai, *J Energy Storage*, 21 (2019) 618.
13. C. J. Xu, L. Weng, L. Ji and J. Q. Zhou, *Eur J Mech a-Solid*, 73 (2019) 47.
14. R. Xiong, J. P. Tian, W. X. Shen and F. C. Sun, *Ieee T Veh Technol.*, 68 (2019) 4130.
15. Z. Xu, S. Mandal, J. Y. Gao, H. Surdi, W. W. Li, Y. Yamaoka, G. X. Piao, T. Tabuchi, H. R. Li, K. Matsumoto and S. Chowdhury, *Ieee T Electron Dev.*, 65 (2018) 5301.
16. Y. Zhao, P. Stein, Y. Bai, M. Al-Siraj, Y. Y. W. Yang and B. X. Xu, *J Power Sources*, 413 (2019) 259.
17. B. Wu and W. Lu, *J. Mech. Phys. Solids*, 125 (2019) 89.
18. N. Weber, S. Landgraf, K. Mushtaq, M. Nimtz, P. Personnettaz, T. Weier, J. Zhao and D. Sadoway, *Electrochimica Acta*, 318 (2019) 857.
19. R. X. Zhao, P. J. Kollmeyer, R. D. Lorenz and T. M. Jahns, *Ieee T Ind App.l*, 55 (2019) 1922.
20. C. Zelger, M. Sussenbacher, A. Laskos and B. Gollas, *J Power Sources*, 424 (2019) 76.
21. J. S. Yu, W. Q. Tang, D. Y. Tang, J. Q. Wan and J. J. Liu, *J Amb Intel Hum Comp.*, 10 (2019) 923.
22. S. G. Yao, Y. H. Zhao, X. F. Sun, Q. Zhao and J. Cheng, *Electrochimica Acta*, 307 (2019) 573.
23. M. Ye, X. Song, R. Xiong and F. C. Sun, *Ieee Access*, 7 (2019) 14256.
24. S. Yang, W. W. Wang, C. Lin, W. X. Shen and Y. D. Li, *Energy*, 185 (2019) 202.

25. J. B. Yang, X. H. Xu, Y. Q. Peng, J. Y. Zhang and P. Y. Song, *Energy*, 183 (2019) 1123.
26. F. F. Yang, X. B. Song, F. Xu and K. L. Tsui, *Ieee Access*, 7 (2019) 53792.
27. F. F. Yang, X. B. Song, G. Z. Dong and K. L. Tsui, *Energy*, 171 (2019) 1173.
28. G. Sierra, M. Orchard, K. Goebel and C. Kulkarni, *Reliab. Eng. Syst. Saf.*, 182 (2019) 166.
29. Z. M. Xi, M. Dahmardeh, B. Xia, Y. H. Fu and C. Mi, *Ieee T Veh Technol.*, 68 (2019) 8613.
30. W. Z. Yan, B. Zhang, G. Q. Zhao, S. J. Tang, G. X. Niu and X. F. Wang, *Ieee T Ind Electron.*, 66 (2019) 3227.
31. G. Z. Dong, Z. H. Chen and J. W. Wei, *Ieee T Ind Electron.*, 66 (2019) 8533.
32. D. Y. Huang, Z. Chen, C. W. Zheng and H. B. Li, *Energy*, 185 (2019) 847.
33. C. Chen, R. Xiong, R. X. Yang, W. X. Shen and F. C. Sun, *J Clean Prod.*, 234 (2019) 1153.
34. T. Yamanaka, Y. Takagishi, Y. Tozuka and T. Yamaue, *J Power Sources*, 416 (2019) 132.
35. X. D. Xu, C. Q. Yu, S. J. Tang, X. Y. Sun, X. S. Si and L. F. Wu, *Ieee Access*, 7 (2019) 105186.
36. J. H. Meng, D. I. Stroe, M. Ricco, G. Z. Luo and R. Teodorescu, *Ieee T Ind Electron.*, 66 (2019) 7717.
37. S. L. Wang, J. Y. Shi, C. Fernandez, C. Y. Zou, D. K. Bai and J. C. Li, *Energy Sci Eng.*, 7 (2019) 546.
38. R. G. Wang, X. N. Zhang and J. Bao, *J Process Contr.*, 73 (2019) 9.
39. G. A. Liu, C. Xu, H. M. Li, K. Jiang and K. L. Wang, *Appl Energ*, 250 (2019) 677.
40. L. M. Wang, J. Y. Niu, W. Zhao, G. C. Li and X. L. Zhao, *Int J Energ Res.*, 43 (2019) 2086.
41. H. Y. Wang, Y. Y. Fan, C. Chen, T. Tao and Z. Y. Qiao, *Iet Circ Device Syst.*, 13 (2019) 245.
42. A. Trovo, G. Marini, A. Sutto, P. Motto, M. Giomo, F. Moro and M. Guarnieri, *Appl Energ*, 240 (2019) 893.
43. S. B. Xie, X. S. Hu, S. W. Qi, X. L. Tang, K. Lang, Z. K. Xin and J. Brighton, *Energy*, 173 (2019) 667.
44. B. Xiao, Y. G. Liu and B. Xiao, *Ieee Access*, 7 (2019) 54192.
45. J. P. Tian, R. Xiong and Q. Q. Yu, *Ieee T Ind Electron.*, 66 (2019) 1576.
46. X. P. Tang, Y. J. Wang, C. F. Zou, K. Yao, Y. X. Xia and F. R. Gao, *Energ Convers Manage*, 180 (2019) 162.
47. J. Su, M. Lin, S. L. Wang, J. Li, J. Coffie-Ken and F. Xie, *Meas. Control*, 52 (2019) 193.
48. T. Morstyn, A. V. Savkin, B. Hredzak and V. G. Agelidis, *Ieee T Smart Grid*, 9 (2018) 4735.
49. X. D. Wang, L. W. Xu, P. Fu, Y. A. Wu, H. F. Mao and J. Li, *Ieee T Plasma Sci.*, 46 (2018) 1658.
50. T. Dong, P. Peng and F. M. Jiang, *Int. J. Heat Mass Transfer*, 117 (2018) 261.
51. S. Maslan, M. Sira, V. N. Zachovalova and J. Streit, *Ieee T Instrum Meas.*, 66 (2017) 1355.
52. Z. G. C. Taskiran, U. E. Ayten and H. Sedef, *Circ Syst Signal Pr*, 38 (2019) 26.
53. C. C. Yuan, B. J. Wang, H. Z. Zhang, C. Long and H. H. Li, *Int. J. Electrochem. Sci.*, 13 (2018) 1131.
54. Z. B. Wei, J. Y. Zhao, C. F. Zou, T. M. Lim and K. J. Tseng, *J Power Sources*, 402 (2018) 189.
55. S. Wang, C. Fernandez, C. Yu, Y. Fan, W. Cao and D.-I. Stroe, *J Power Sources*, 471 (2020) 228450.
56. Z. B. Wei, R. Xiong, T. M. Lim, S. J. Meng and M. Skyllas-Kazacos, *J Power Sources*, 402 (2018) 252.
57. J. Wang, R. Xiong, L. L. Li and Y. Fang, *Appl Energy*, 229 (2018) 648.
58. S. Wang, D.-I. Stroe, C. Fernandez, C. Yu, C. Zou and X. Li, *J Power Sources*, 450 (2020) 227652.
59. X. Xin, S. L. Wang, C. M. Yu, J. Cong and J. Coffie-Ken, *Int. J. Electrochem. Sci.*, 15 (2020) 2226.
60. Y. W. Wang, J. M. Jiang, Y. H. Chung, W. C. Chen and C. M. Shu, *J. Therm. Anal. Calorim.*, 135 (2019) 2891.